ELSEVIER

Journal of Molecular Structure (Theochem) 389 (1997) 203–216

THEO CHEM

Quantum decoherence: a consistent histories treatment of condensed-phase non-adiabatic quantum molecular dynamics[1]

Eric R. Bittner[a], Benjamin J. Schwartz[b], Peter J. Rossky[a,*]

[a]*Department of Chemistry and Biochemistry, University of Texas at Austin, Austin, TX 78712-1167, USA*
[b]*Institute for Polymers and Organic Solids, University of California at Santa Barbara, Santa Barbara, CA 93106-5090, USA*

Received 1 November 1995; accepted 29 March 1996

Abstract

We address the issue of quantum decoherence in mixed quantum classical simulations. We demonstrate that restricting the bath paths to a single stationary path which connects an initial quantum state to a final quantum state affects a coarse graining of the quantum subspace which leads to a macroscopic loss of quantum coherence. The coarse graining can be described in terms of reduction mappings of the density matrix of the reduced quantum system + stationary bath path. Application of the present model to various prototypical condensed-phase chemical problems reveals that non-adiabaticity is extremely sensitive to the decoherence timescale. Furthermore, we derive how to obtain quantum coherence timescales from realistic mixed quantum classical simulations and use this information to compute the non-radiative lifetimes for an excess electron in H_2O and D_2O. We demonstrate that subtle differences in the quantum coherence times provide a rationalization for a long-standing puzzle regarding the lack of experimentally observed isotopic dependence of the non-radiative lifetime of a photoexcited electron in H_2O and D_2O.

Keywords: Quantum decoherence; Non-adiabatic transition; Mixed quantum classical system; Decoherent histories

1. Introduction

In computer simulations of condensed-phase chemical processes it is often desirable to partition the system into a few select degrees of freedom which are treated explicitly by quantum mechanics while treating the remainder as classical or quasiclassical variables.[2] In these simulations, the quasiclassical variables are used to generate a potential energy surface which defines the eigenstates of the quantum system for a given configuration. These states in turn define the potential surfaces which govern the motion of the quasiclassical variables. Under the Born–Oppenheimer approximation, the quantum states follow the classical variables adiabatically and no transitions occur between the quantum states. However, transitions in the quantum system occur when the adiabaticity conditions can no longer be satisfied, such as when the classical motion becomes very fast relative to the quantum evolution or the quantum energy levels become nearly degenerate. Such non-adiabatic or radiationless transition mechanisms play fundamental roles in many chemical

* Corresponding author.

[1] Presented at the 2nd Electronic Conference on Computational Chemistry, November 1995. This issue along with any supplimentary material can be accessed from the THEOCHEM HomePage at URL:http://www.elsevier.nl/locate/theochem.

[2] The literature on mixed quantum classical molecular dynamics simulations is enormous: see for example [1](a). For some recently developed adiabatic methods see [1](b).

PII S0166-1280(96)04612-X

and biological processes. There has been a great deal of discussion of non-adiabatic dynamical algorithms and their importance to chemical reaction dynamics in the literature, which we make no attempt to review here (see [2](a) for a recent review). For a few recent examples of non-adiabatic dynamical calculations, see [2](b). The role of adiabaticity in biomolecular electron transfer reactions is explored in [3].

Questions regarding the validity of the partitioning between quantum and classically described variables arise when one is forced to consider phase interference effects between alternative paths which the bath variables may take over the course of the simulation [4,5]. (For a discussion of quantum coherence and adiabaticity in the condensed phase see [4].) On longer timescales, there should be no interference between alternative paths and the results from the alternative paths can be treated as ordinary probabilities. However, on short timescales, phase coherences between alternative paths are extremely important and affect short time transition probabilities due to constructive and destructive interferences. In the condensed phase, the rapid temporal decay of these phase coherences, known as quantum decoherence, severely limits the formation of long-lived quantum superposition states and hence plays an important role in the determination of the transition probability between two states. Amongst the key issues at hand is the identification of the appropriate timescales which allow a perfectly classical treatment of the bath dynamics in which no phase interferences between alternative paths are considered.

In the mixed quantum classical computational methods for including non-adiabatic transitions in molecular dynamics-type simulations developed most notably by Tully [6,7], Webster, Rossky and co-workers [8–10], and most recently by Coker and co-workers [11], the classical variables describing the surrounding bath are allowed to "switch" or "hop" between different adiabatic potential energy surfaces according to a random selection criteria based upon the propagation of the quantum amplitudes for each adiabatic quantum state. In the methods used by Tully [6,7] and Coker [11], these coherences are retained throughout the course of the simulation, whereas in the method of Webster and co-workers [8,9] a finite computational coherence time is placed on the quantum variables (typically one molecular dynamics time step). A complete discussion of the merits of each method is beyond the scope of this paper and each method has been sufficiently described in the literature.

Recently, we presented a theory of quantum decoherence suitable for mixed quantum classical systems and numerical examples of the effect of quantum coherence in a variety of model physical systems [5]. Starting from the theory of decoherent histories [12–16] we derived a quantum master equation suitable for mixed quantum classical systems which included a coherence timescale as an input parameter. By varying the decoherence time we demonstrated the profound effect decoherence has on a wide variety of condensed-phase chemical processes involving non-adiabatic transitions.

What is needed is a robust a priori or dynamical estimation of the quantum coherence timescale and the purpose of this paper is to provide the formal mechanism for doing this. Other recent work toward this goal has been presented by Okazaki et al. [17] using higher-order moments of the density matrix and an extension of the path integral influence functional method in which the quantum bath is treated implicitly.

Here we present an overview of our current theory of quantum decoherence and its implementation in explicit mixed quantum classical molecular dynamics treatments of condensed-phase phenomena. We also present sample calculations aimed at understanding the role of decoherence in the non-radiative relaxation of photoexcited species. Examples include a model two-level chemical system as well as simulations of an excess electron in H_2O and D_2O.

2. Decoherent histories

Our formal analysis stems from the decoherent histories theory by Griffiths [12], Omnés [14] and Gell-Mann and Hartle [15,16] who were interested in elucidating the physical origins of the classical domain in the context of a closed quantum system, such as the entire universe. The key element in this theory is the notion of histories. Simply stated, a history is a sequence of quantum mechanical projections which occur at successive moments in time. We

define Z as the space of all possible paths (of the combined "system" and "bath") which connect an initial state, $Q_{\circ}$, to a final state, Q_f. We shall label the adiabatic quantum states by α_j and the bath variables by x. Thus, the initial and final states are completely specified by a set of quantum states and a bath configuration: $Q = Q(\alpha,x)$. The paths connecting the initial and final states are completely fine grained since the values of all the paths can be specified at all times along the course of the path. The fundamental property of quantum mechanics is that one cannot assign a probability to a completely fine-grained path, only an amplitude. Making predictions (i.e. measurements) or restricting the space of paths to particular subspaces imposes coarse graining on the space of paths and coarse-grained sets of paths are added according to the ordinary rules of adding probabilities. In short, completely fine-grained paths are added as amplitudes – which is the typical "sum over Feynman paths" picture for constructing the transition matrix between the initial and final states, and coarse-grained sets of paths are added as probabilities.

Sets of histories are obtained by partitioning the unit operator into projectors, $\mathcal{P}_\alpha$, at various moments in time. In the simulations which we describe later, this corresponds to the restriction of the paths taken by the bath variables to their stationary phase (i.e. classical) paths, $x_{cl}(t)$. The quantum paths are thus restricted as those which follow $x_{cl}(t)$. Thus, coarse graining is over the the entire space of system–bath paths. The projection operators satisfy the orthonormality conditions

$$\mathcal{P}_\alpha \mathcal{P}_\beta = \delta_{\alpha\beta} \tag{1}$$

$$\sum_\alpha \mathcal{P}_\alpha = 1 \tag{2}$$

The time development of projectors is given in the Heisenberg representation as

$$\mathcal{P}_\alpha(t) = e^{+iHt}\mathcal{P}_\alpha e^{-iHt} \tag{3}$$

Thus defined, we can write an element of the set of histories as a string of N projections at various points in time

$$C_\alpha(x) = \mathcal{P}_{\alpha_N}(x_N)\cdots\mathcal{P}_{\alpha_2}(x_2)\mathcal{P}_{\alpha_1}(x_1) \tag{4}$$

In other words, at time t_1 we projected the combined system onto quantum state α_1 with bath configuration x_1, at time t_2 we projected the quantum subsystem onto adiabatic state α_2 with bath configuration x_2, and so forth.

The Borel measure of the space of histories is given by

$$p(C_\alpha) = \mathrm{tr}[C_\alpha \rho_\circ C_\alpha] \tag{5}$$

where $\rho_\circ$ is the density matrix at time $t_\circ$. This measure can be interpreted as a probability only when the standard summation rules for adding probabilities can be satisfied. The space of histories which satisfies this criteria has been termed consistent or decoherent by Gell-Mann and Hartle [15,16]. Whether a pair of histories is decoherent or consistent is determined by the decoherence functional

$$D[\alpha,\alpha'] = \mathrm{tr}[C_\alpha \rho_\circ C_{\alpha'}] \tag{6}$$

The sum rules for adding histories as probabilities is satisfied when the consistency criteria

$$Re\{D[\alpha,\alpha']\} = 0 \tag{7}$$

True decoherence requires satisfaction of the stronger condition

$$D[\alpha,\alpha'] = 0 \tag{8}$$

although, for purposes in condensed-phase quantum mechanics, the two conditions are essentially equivalent.

In mixed quantum classical simulations, quantum mechanical histories are generated as the quasiclassical variables are allowed to switch between the adiabatic potential energy surfaces. Let us define the history label, α, as a series of quantum state indices which indicate which state the quantum system was in at a particular moment in time. In other words $\alpha = \{\alpha_1, \alpha_2, ..., \alpha_i, ...\}$ says that at some intermediate time, t_i, the quantum subsystem was determined to be in state α_i. Furthermore, we label the quasiclassical path associated with this sequence as $x^\alpha(t)$ which has end-points $x_\circ$ at some initial time and $x_n^{\alpha_n}$ at some later time t_n. Alternative histories arise naturally in the surface hopping picture since the intermediate quantum states are chosen randomly at each time interval according to an appropriate selection criteria leading to bifurcations in the classical paths. Each bifurcation corresponds to a different choice of quantum state at the intermediate time. An illustration of this is shown in Fig. 1. Thus, the projection operators

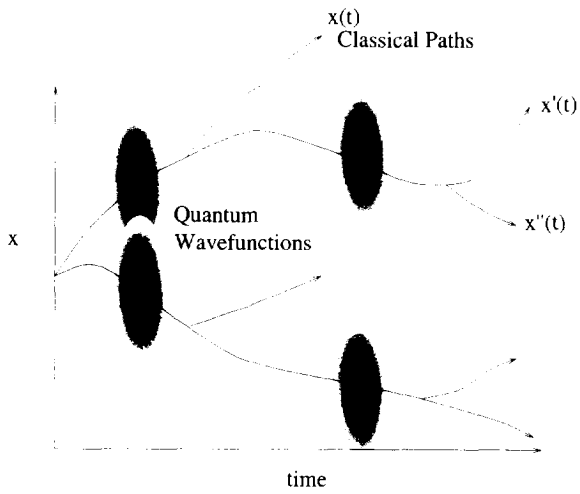

Fig. 1. Illustration of coarse graining. Shown in schematic form is the time evolution of system wavefunction along various alternative stationary phase paths, of the bath, $x(t)$. Bifurcations in the classical paths occur at various times due to discrete transitions in the quantum system. Formally, these occur continuously along a given bath trajectory; however, in simulations they can occur as stochastic events. As the classical paths diverge, the overlap between alternative bath wavefunctions is decreased and coarse graining is accomplished. The implication of this is that the quantum state associated with the classical path labeled $x(t)$ will not be coherent with the state associated with $x''(t)$ and will only remain partially coherent with the state associated with its branch pair, x', for a finite period of time.

described above project out a single classical trajectory and an adiabatic state at each time increment and a history is constructed by recording which adiabatic quantum state the classical path visited at each time. The decoherence functional tells us the relative quantum mechanical phase coherence between pairs of alternative histories at a given time.

2.1. Determining the decoherence timescale via simulations

In order to further illustrate the concepts behind the consistent histories method, let us consider the decoherence between two alternative branches over a short time interval following a hopping selection. We begin by setting the initial quantum state, $\phi_\circ$, to be an eigenstate of the adiabatic Hamiltonian $H(x_\circ)$ where $x_\circ$ is the initial classical configuration. Next, we propagate this state forward in time to time t_1:

$$\phi_\circ(x_\circ) \rightarrow \sum_{\alpha_1} c_{\alpha_1} \phi^1_{\alpha_1}(x_1^{\alpha_1}) \tag{9}$$

The propagated wave is of course a superposition of alternative states and the coefficients $\{c_{\alpha 1}\}$ are the complex amplitude coefficients. The paths taken by the classical particles which connect the initial configuration $x_\circ$ to the final configurations $\{x_1^{\alpha_1}\}$ are labeled by the selected quantum state at the end of the time step. In essence, each alternative classical path evolves on a different adiabatic potential energy surface corresponding to a different adiabatic eigenstate.[3] In order to provide a measure for the decoherence, we need a representation of the entire system–bath wavefunction for a given classical configuration. This is accomplished by assigning to each classical particle a Gaussian coherent state wavefunction centered about the instantaneous phase space coordinates $\{x(t),p(t)\}$. Thus, we approximate the total wavefunction for any classical configuration as

$$|\phi_n^\alpha(x_n^\alpha)\rangle = |\phi_n^\alpha\rangle|z_n^\alpha\rangle \tag{10}$$

where $z_n^\alpha = (1/a)(x_n^\alpha + ip_n^\alpha/a)$ is a collective dimensionless variable on the complex plane. Using this assumption, the decoherence functional becomes

$$\begin{aligned} D[\alpha_1\alpha_1'] = {} & \langle z_1^{\alpha_1}|\langle\phi_1^{\alpha_1}(x_1^{\alpha_1})|\exp\left[-i\int_{t_\circ}^{t_1} ds H(x_1^{\alpha_1}(s))\right] \\ & \times |\phi_\circ(x_\circ)\rangle|z_\circ\rangle\langle\phi_\circ(x_\circ)|\langle z_\circ| \\ & \times \exp\left[+i\int_{t_\circ}^{t_1} ds H(x_1^{\alpha_1'}(s))\right]|\phi^{\alpha_1'}(x_1^{\alpha_1'})\rangle|z_1^{\alpha_1'}\rangle \end{aligned} \tag{11}$$

If we make the approximation that on short timescales the nuclear wavefunction does not disperse, we can invoke a "frozen Gaussian" approximation and let the coherent states follow the classical paths [19]. Thus, using the coherent state displacement operator

$$\hat{D}(z) = \exp[z\hat{a}^\dagger - z^*\hat{a}] \tag{12}$$

the decoherence functional becomes

$$\begin{aligned} D[\alpha,\alpha'] \approx {} & \langle z_1^{\alpha_1}|\hat{D}(z_1^{\alpha_1}(t))|z_\circ\rangle\langle z_\circ|\hat{D}^\dagger(z_1^{\alpha_1'}(t))|z_1^{\alpha_1'}\rangle \\ & \times \exp\left[+i(S[z_1^{\alpha_1}(t)] - S[z_1^{\alpha_1'}(t)])\right] \\ & \times T_{\alpha_1}(x_1^{\alpha_1}(t))T^\dagger_{\alpha_1'}(x_1^{\alpha_1'}(t)) \end{aligned} \tag{13}$$

$$\approx J(t)T_{\alpha_1}(x_1^{\alpha_1}(t))T^\dagger_{\alpha_1'}(x_1^{\alpha_1'}(t)) \tag{14}$$

where $\hat{a}$ and $\hat{a}^\dagger$ are harmonic oscillator annihilation

[3] As a technical note, restricting the classical evolution to a single adiabatic surface with sudden hops between surface is problematic since it lacks self-consistency at the transition [8]. A more precise description of the potential is given by Pechukas [18].

and creation operators. The displacement operator continuously shifts the centroid of the Gaussian wave from its initial phase space position along the classical trajectory to the final position. Finally, $S[x_1^{\alpha_1}(t)]$ is the action along the classical path $x_1^{\alpha_1}(t)$, which connects the initial point $x_\circ$ to the final point $x_1^{\alpha_1}$ when the quantum subsystem makes the transition from the initial adiabatic state $|\phi_\circ^{\alpha_\circ}\rangle$ to the adiabatic state $|\phi_1^{\alpha_1}\rangle$ at time t_1.

$$S[x^{\alpha_1}(t)] = \int_{t_\circ}^{t_1} \mathrm{d}s \frac{1}{2} m(\dot{x}^{\alpha_1}(t))^2 \tag{15}$$

and $T_{\alpha_1}(x_1^{\alpha_1}(t))$ is the quantum transition matrix element,

$$T_{\alpha_1}[x^{\alpha_1}(t)] = \langle \phi_1^{\alpha_1}(x_1^{\alpha_1}| \exp\left[-\mathrm{i} \int_{t_\circ}^{t_1} \mathrm{d}s H[x_1^{\alpha_1}(t)] \right] |\phi_\circ(x_\circ)\rangle \tag{16}$$

both are functionals computed along the classical trajectory $x_1^{\alpha_1}(t)$.

The classical paths are the stationary paths $x^{\alpha_1}(t)$ between the initial and final end-points when the quantum subsystem makes a transition from the initial state to the final (i.e. post-selected) state [8,9,18]. The corresponding potential is

$$V_Q[x(t)] = Re\left\{ \frac{\langle \phi^{\alpha_1}(x^{\alpha_1})|U^\dagger(t_1,t)H(x^{\alpha_1}(t))U(t,t_\circ)|\phi_\circ\rangle}{U(t_1,t_\circ)} \right\} \tag{17}$$

Here, the potential and force acting on the classical variables at an intermediate time $t_\circ < t < t_1$ is computed by back propagating the final state and forward propagating the initial state to the intermediate time. Variational methods based upon earlier work by Pechukas [18] for computing the stationary phase paths have been presented by Webster and co-workers [8,9] and by Coker and Xiao [11].

In Eq. (14), $J(t)$ describes the overlap between the propagated bath wavefunctions for each alternative trajectory with the initial state. The two terms comprising $J(t)$ can be combined using the identity for the scalar product of coherent states

$$\begin{aligned} J(t) &= \langle z_1^{\alpha_1}|\hat{D}(z_1^{\alpha_1}(t))|z_\circ\rangle\langle z_\circ|\hat{D}^\dagger(z_1^{\alpha_1'}(t))|z_1^{\alpha_1'}\rangle \\ &= \exp\left[-\frac{1}{2}|z_1^{\alpha_1}(t) - z_1^{\alpha_1'}(t)|^2 - z_1^{\alpha_1}(t)(z_1^{\alpha_1'}(t))^* \right. \\ &\quad \left. - z_1^{\alpha_1'}(t)(z_1^{\alpha_1}(t))^* \right] \end{aligned} \tag{18}$$

producing a term which gives the overlap between alternative bath states. This becomes clear when written in terms of the classical variables x, p. In order to avoid cluttered notation, we shall use the abbreviations $x(t) = x^{\alpha_1}(t)$ and $x'(t) = x_1^{\alpha_1'}(t)$ for the alternate sets of bath variables. Thus

$$\begin{aligned} J(t) = \exp\Big[&-\frac{a}{2}(x(t)-x'(t))^2 - \frac{1}{2a}(p(t)-p'(t))^2 \\ &+ \mathrm{i}(x(t)-x'(t))(p(t)+p'(t))\Big] \end{aligned} \tag{19}$$

The width parameter thus far has been left arbitrary and various criteria can be invoked. However, rigorous analysis of the non-adiabatic transition rate between displaced harmonic oscillators in the high-temperature limit indicates that the optimal width is found by setting [20,21]

$$a = \frac{6MkT}{\hbar^2} \tag{20}$$

We used this as a criterion for setting the Gaussian widths in the calculations presented below.

We can simplify matters further by recognizing that the decoherence functional converges to zero very rapidly and that to leading order, the decay envelop is Gaussian in form. Thus motivated, we approximate the classical evolution by Taylor expansion of the stationary path about an initial starting configuration, $\{x_\circ, p_\circ\}$.

$$x(t) \approx x_\circ + \dot{x}_\circ t - \frac{t^2}{2M} f_\alpha(x_\circ)\cdots \tag{21}$$

$$p(t) \approx p_\circ - t f_\alpha(x_\circ)\cdots \tag{22}$$

where the force, $f_\alpha(x)$, is approximated from the adiabatic potential at $x_\circ$, using the Hellmann–Feynman theorem [22,23]

$$f_\alpha(x_\circ) = \langle \phi_\alpha(x_\circ)| \frac{\partial H(x_\circ)}{\partial x} |\phi_\alpha(x_\circ)\rangle \tag{23}$$

where $H(x_\circ)$ is the quantum (electronic) Hamiltonian evaluated at the initial classical configuration, $x_\circ$.

Thus, to leading order ($O(t^2)$), the nuclear overlap contribution to the decoherence functional is approximately given by

$$J(t) \approx \left\langle \exp\left[-t^2 \frac{(f_\alpha(x_\circ) - f_{\alpha'}(x_\circ))^2}{2a} \right] \right\rangle \tag{24}$$

where the cosine term is the real part of the action contribution evaluated in the short time approximation. This modulates the overlap integral at the frequency of the energy difference between the different adiabatic electronic states. Finally, we average over a canonical ensemble of initial configurations to produce $J(t)$ curves for a given physical system. From these we can determine the characteristic decoherence timescales for these systems.

3. Model calculations

3.1. Non-adiabatic relaxation of excited states

In order to elucidate the role of coherence loss in a prototypical chemical process, we consider the problem of a classical Brownian harmonic oscillator coupled to two electronic states. This is a classic problem in chemical physics since chemical reactions are associated with a change in the configuration of both the electronic structure and the nuclear configuration of the reactants. In this example, we consider the case in which the Hamiltonian consists of a reaction coordinate x coupled to a harmonic bath with coordinates $\{q_n\}$ and coupled to a two-electronic level system, i.e. the Hamiltonian is given by

$$H = H_{\circ} + \sum_n \frac{m_n}{2}\dot{q}_n^2 + \frac{m_n\omega_n^2}{2}\left(q_n - x\frac{c_n}{\omega_n^2 m_n}\right)^2 \tag{25}$$

and

$$H_{\circ} = \frac{p^2}{2m} + E_{\pm}(x) - \sum_n \frac{c_n^2}{2m_n\omega_n^2}x^2 \tag{26}$$

The explicit dependence on the bath can be eliminated by introducing the spectral density

$$J(\omega) = \frac{\pi}{2}\sum_n \frac{c_j^2}{m_j\omega_j}\delta(\omega - \omega_j) \tag{27}$$

For the ohmic case where $J(\omega) = m\omega\gamma_{\circ}$, the classical variable, x, evolves according to the classical Langevin equation

$$m\dot{x} = -V_{\pm}'(t) - \gamma_{\circ}\dot{x} + \zeta(t) \tag{28}$$

where $\zeta(t)$ is Gaussian random variable, $\gamma_{\circ}$ is the damping constant, and $V_{\pm}(t)$ is the adiabatic potential curve.

Here we examine a model photophysics problem in which the initial state is prepared in the ground vibrational state of the lowest electronic state, $|G,n = 0\rangle$, and is excited via a short laser pulse to the first excited electronic state. Following excitation, the vibrational wavepacket evolves on the excited state adiabatic potential surface. For short times, we can approximate the nuclear motion using coherent state wavepackets which follow the classical motion. Since the nuclear motion is effectively coupled to the bath modes, the centroid evolution of the coherent state will be given by a generalized Langevin equation. Over the course of the nuclear evolution on the excited adiabatic surface, the nuclear wavepacket will traverse a region of strong coupling between the excited and ground electronic states and can induce electronic transitions back to the ground electronic state.

The diabatic curves and couplings are given by

$$V_i(x) = \frac{m\omega_i}{2}(x - x_i)^2 + bx \quad \text{where } i = 1, 2 \tag{29}$$

$$V_{12}(x) = c\exp(-dx^2) \tag{30}$$

The potential parameters for Eq. (30) are for a symmetric double well potential and are as follows: $\omega_1 = \omega_2 = 300\ \text{cm}^{-1}$, $b = 0$, $c = 900\ \text{cm}^{-1}$, $d = 1.0$ Å, $x_c = 0.5$ Å. The energy gap at $x = 0$ is $\Delta E = 1825\ \text{cm}^{-1}$. In each case the nuclear friction constant was $\gamma = 0.1\ \text{cm}^{-1}$.

Our calculations proceed as follows. At time zero, the ground vibrational state of the ground electronic state in the left-hand well is promoted to the excited electronic state. The nuclear vibrational motion is treated via the Langevin dynamics described above and the electronic amplitudes are propagated via the non-adiabatic Schrödinger equation.

$$i\frac{\partial}{\partial t}\phi(x;t) = \left(E^{A}(x;t) + V^{NA}(x;t)\right)\phi(x;t) \tag{31}$$

The diagonal elements, $E^{A}(x;t)$, are simply the adiabatic eigenvalues computed when the nuclear variable is at position x. The off-diagonal terms are the non-adiabatic coupling matrix elements given explicitly by

$$V_{12}^{NA}(x;t) = i\dot{x}\langle\phi_1(x)|\frac{\partial}{\partial x}|\phi_2(x)\rangle \tag{32}$$

Electronic transitions were counted whenever the nuclear motion "switched" between electronic energy surfaces. These switches were computed by

comparing the probability to make a switch to a uniformly distributed random variable at each time step. In other words, for a two-level problem, the probability, $p_{ij}(\delta t)$, to switch between state i to state j over a time interval δt is given by

$$p_{ij}(\delta t) = \frac{2}{\hbar}\frac{\delta t}{\rho_{ij}} Re[\rho_{ij}^* V_{ij}^{NA}]\Theta(-Re[\rho_{ij}^* V_{ij}^{NA}]) \quad (33)$$

where ρ_{ii} and ρ_{ij} are elements of the electronic density matrix and represent the initial electronic population and the phase coherence between the initial and final electronic states. $\Theta(x)$ is the Heaviside step function which insures that the nuclear variables undergo the fewest number of switches between adiabatic states [7].

Quantum decoherence is introduced by periodically reducing the quantum (electronic) wavefunction onto a single adiabatic state using the projection operator methods discussed above. In other words, at various points in time, we resolve the quantum wavefunction (which is a coherent superposition of adiabatic states) into its components and then selecte only one of those components as the new wavefunction (see Fig. 2). This reduction mapping procedure is discussed in greater detail by Bittner and Rossky [5]. As demonstrated in [5], when the time intervals between the projections or reduction mappings are distributed according to a Poisson deviate, the resulting equations of motion for the quantum density matrix is identical

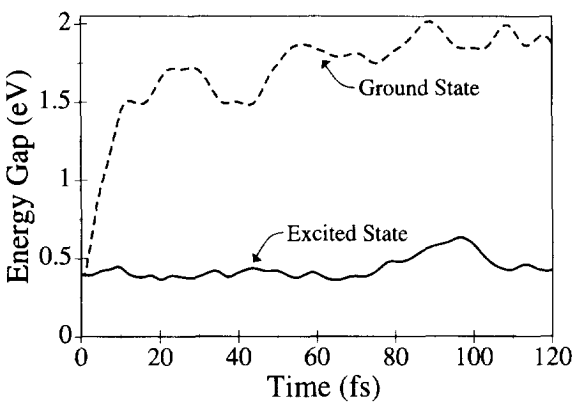

Fig. 2. Survival of excited state as a function of coherence timescales. Decreasing the quantum coherence timescale inhibits the formation of sufficiently long-lived coherences between the ground and excited states and hence diminishes the non-adiabatic transition probability.

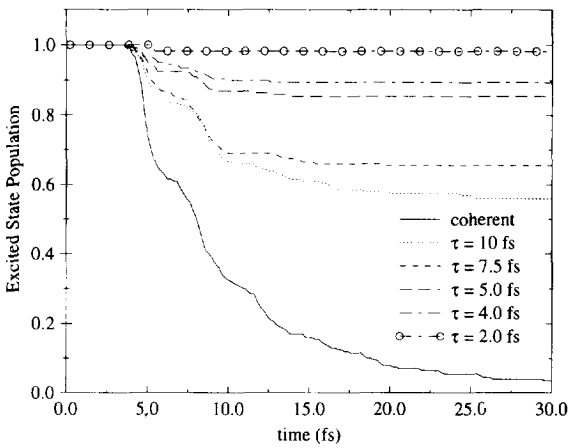

Fig. 3. Divergence of the ground state–excited state energy gap of the hydrated electron for trajectories propagating on the ground versus excited state potential surfaces, starting from the same initial configuration in the equilibrated excited state. The solid curve indicates that continued propagation along the excited state produces little change in the quantum energy gap. The dashed line shows the rapid increase in the quantum energy gap as the electron propagates on the ground state surface, establishing its new equilibrium.

to that of a quantum Brownian oscillator in the absence of dissipative coupling [24,25].

In Fig. 3 we plot the survival probability of the excited electronic state as a function of both time and quantum coherence timescales. Here we plot the distribution of switching times between the excited state surface and the ground state surface as a function of the preselected quantum coherence timescale. As the quantum coherence timescale is decreased from infinity (i.e. purely coherent electronic dynamics) to very short (2 fs), the lifetime of the excited state increases dramatically showing the profound sensitivity of the survival to the choice of coherence timescales in this very simple model. This reason for this dramatic effect can be explained by a cursory glance back at the switching probability in Eq. (33) above. Since the reduction of the wavefunction from a superposition state to pure eigenstate destroys any coherences between the eigenstates (i.e. $\rho_{ij} \rightarrow 0$ for $i \neq j$), the probability to make a transition is diminished because an insufficient amount of transition amplitude has been allowed to accumulate. Indeed, when the quantum coherence timescale is much shorter than the "bare" non-adiabatic transition rate, the system can effectively become "trapped" for long periods of time in the excited state. This "quantum Zeno" effect

or "quantum watched pot" effect has profound implications for a number of physical systems which undergo nonradiative relaxation process. One such system is discussed next.

3.2. Non-adiabatic relaxation of an excess electron in water

In this example we examine another prototypical system: the hydrated electron. Because the hydrated electron has only a single quantum degree of freedom, namely the quantized cavity modes of the excess electron itself, which is strongly coupled with the nuclear motions of the surrounding bath, the hydrated electron provides an excellent testing ground for models of non-radiative relaxation in the condensed phase [8,20,21,26–34]. The large optical cross-section of the hydrated electron also makes it amenable to spectroscopic investigation [35–41]. With the advent of femtosecond laser techniques and the development of non-adiabatic dynamical algorithms such as those described above, the hydrated electron has provided the first condensed system where non-adiabatic theory and experiment have successfully converged [42].

Interest in the non-adiabatic dynamics of the hydrated electron was originally spurred by femtosecond experiments studying the formation of equilibrium hydrated electrons following multiphoton ionization of neat water [37,38]. While the mechanism of electron production in these experiments is not fully understood [40,41], it is clear that the formation of the equilibrium species takes place by an essentially two-state process. The kinetic picture [33] that emerged from the combination of these experiments [37,38], adiabatic simulations [34] and non-adiabatic calculations [8,31] points to trapping of the electron in the lowest excited state (sometimes referred to as the "wet" electron) followed by non-adiabatic relaxation to the ground state (the equilibrium "solvated" electron). Formation of the excited state electron from the initially produced species was found to take 110–240 fs [37,38]. The non-adiabatic relaxation time for the electron determined in these experiments is 250–500 fs [37,38]. Investigations of this process in deuterated water have shown that the isotope effect on the non-adiabatic transition rate is at most a few per cent [39].

More recent experiments [35,36] and quantum simulations [26,29,30,32] have investigated the non-adiabatic dynamics of the hydrated electron by photoexciting the equilibrium ground state species and monitoring the subsequent solvation of the excited state and its internal conversion back to the ground state. Upon photoexcitation, the quantum energy gap of the hydrated electron starts at its equilibrium ground state value and continuously decreases with time as the excited state charge distribution is solvated. The non-adiabatic coupling between the two states increases as the gap becomes smaller, leading to an increasing non-adiabatic transition rate with time [29]. The excited state solvation time for the photoexcited electron is 250–300 fs, and the non-adiabatic transition rate from the equilibrated excited state is of the order of 1 ps^{-1} [29,35]. Experiments in D_2O show identical spectral dynamics, indicating little isotope effect on either the solvation dynamics or the non-adiabatic transition rate [35]. Here we utilize non-adiabatic mixed quantum classical molecular dynamics in a large-scale simulation to investigate the origins of quantum decoherence in this prototypical condensed-phase system.

The simulation techniques employed are identical to those used in earlier work by Murphrey and Rossky [8,31], studying the relaxation of electrons photoinjected into neat water, as well as the present case of photoexcitation of equilibrium hydrated electrons by Schwartz and Rossky [29,30]. Briefly, the model consists of 200 classical SPC water molecules with the addition of internal flexibility [43] and one quantum electron in a cubic cell of side 18.17 Å (corresponding to a solvent density of 0.997 g ml^{-1}) with standard periodic boundary conditions at room temperature. The electron–water interactions were described with a pseudo-potential [44] and the equations of motion integrated using the Verlet algorithm with a 1 fs time step in the microcanonical ensemble (see for example [45]). The adiabatic eigenstates at each time step were computed via an efficient iterative and block Lanczos scheme utilizing a 16^3 plane wave basis [8]; the lowest six eigenstates were computed during non-adiabatic molecular dynamics. Twenty configurations in which the energy gap was resonant with the experimental laser frequency [29,35] were chosen from a 35 ps equilibrated ground state run as the starting points for non-equilibrium excited state trajectories. The solvation of the newly formed excited state, non-adiabatic transition times for the 20 trajectories, and a

comparison of ultrafast spectroscopy computed from these simulations to experiment are all available in the literature [29,30]. A detailed microscopic analysis of the non-adiabatic coupling and energy disposal following the internal conversion for these simulations is forthcoming [46].[4,5]

Quantum coherence in these simulations was maintained utilizing the stationary phase surface hopping non-adiabatic dynamics algorithm of Webster and co-workers [8,9]. In these earlier studies of the hydrated electron, we chose to drop coherence at the end of each 1 fs time step; in other words, we do not utilize the complex phases of the quantum transition amplitudes, T_{ij}, over more than one time step. This choice, though arbitrary, was based on expectations that the decoherence time for this system should be of the order of 1 fs. This choice is equivalent to having a rectangular decay of the nuclear function $J(t)$, i.e. $J(t)$ for this algorithm starts at 1 and stays there for 1 fs, and then instantly drops to zero for times greater than 1 fs. A modified version of this algorithm which chooses coherence intervals based on instantaneous values for the quantum decoherence time will allow for dynamics with a more realistic decay of quantum coherence [28]. The rapid divergence of the nuclear positions on the two different surfaces (and hence, choice of a short coherence time) is illustrated conceptually by Fig. 1 . Fig. 2 shows the quantum energy gap for the hydrated electron starting from a configuration equilibrated on the electronic excited state. The solid curve follows the energy gap for continued propagation on the equilibrium excited surface, while the dashed curve shows the gap starting from the same initial configuration but propagating along the ground state surface. Clearly the nuclear configurations giving rise to the quantum energy gap on the different surfaces must diverge rapidly. Thus, the non-adiabatic coupling for this system must be tempered by a short coherence time.

[4] We deliberately avoid using the term "in the first solvation shell" since the excited state hydrated electron is an extended cylindrically symmetric object with a nodal plane in the center. In addition, the electron changes size and shape as solvation proceeds, making it very difficult to rigorously define solvent shells for the electron (see [29,46,47] for more details).

[5] The computed average excited state energy gap, at equilibrium, for the hydrated electron is 0.45 eV with a standard deviation of 0.15 eV.

Using the method outlined above, we can estimate the decay of quantum coherence for the hydrated electron by computing $J(t)$ with information available from the excited state simulations. For the present example, the initial state i is the equilibrium excited state of the hydrated electron, and the final state j is the ground state of the electron. As discussed above, we chose

$$a_n = \frac{6M_n kT}{\hbar^2} \tag{34}$$

for the widths of the frozen Gaussian about the nth atom, which permits a direct comparison with the earlier calculations of Neria and co-workers [20,21]. To compute the equilibrium quantum decoherence which modulates the non-adiabatic transition from the excited state, we take an ensemble average of Eq. (19). Assuming that the excited state was equilibrated at times past 1 ps, we chose 20 configurations at 25–50 fs intervals from each of our 5 longest trajectories for a total of 100 configurations. Since we had already computed the eigenenergies and the excited state Hellmann–Feynman forces on the classical particles for all these configurations, we need only use the eigenfunctions computed previously to determine the Hellmann–Feynman forces along the ground state to obtain an estimate of $J(t)$.

One of the largest puzzles concerning the non-adiabatic dynamics of the hydrated electron has been the surprising lack of a sizable isotope effect on the radiationless transition rate [35,39]. A quick glance at Eq. (32) shows that the nuclear velocities play a direct role in determination of the non-adiabatic transition rate. Since the fastest nuclear velocities in D_2O are classically $\sqrt{2}$ times slower than those in H_2O while the other factors (the electron–water interaction potential, the quantum force on the nuclei, etc.) remain the same between the two solvents, the expectation is that radiationless transition rates should be roughly half as large in D_2O compared to H_2O. Indeed, mixed quantum classical simulations have suggested isotope effects of factors of two to four for the electronic transition rate in this system [20,21,47]. Experiments, however, have found at most a modest difference in the non-adiabatic transition rate for electrons photoinjected into H_2O versus D_2O [39] and no isotopic differences have been observed in the spectroscopic dynamics for photoexcited equilibrium electrons [35].

Here, we explore the possible role of quantum coherence in determining the magnitude of the non-adiabatic transition rate for equilibrium excited state electrons. We find that even though the non-adiabatic coupling is smaller in D_2O than H_2O, a slower decay of quantum decoherence in D_2O allows this smaller coupling to add coherently for a longer time than in H_2O, leading to estimated net electronic transition rates which are comparable in the two solvents.

The simulation techniques we have employed to study the solvated electron in D_2O are essentially identical to those in H_2O, and are described in more detail elsewhere [47]. Briefly, the only differences in simulating the electron in heavy versus light water come in changing the mass of the proton from 1 to 2 amu, and the slight change in solvent density to accurately reflect the experimental density of D_2O at room temperature. In performing these D_2O simulations, carried out prior to the remainder of the present study, we made the choice of a quantum coherence time in the stationary phase surface hopping algorithm of 1 fs, the same as for H_2O. As we will see below, the estimated coherence time in D_2O is roughly 25% longer than that in H_2O. One of the consequences of the hypothesis of equal coherence times is that non-adiabatic trajectories remain on the excited state significantly longer in D_2O, bringing to light a slower component of the solvation response on the $\approx$ 1.2 ps timescale that was not evident in our earlier work [29,30] on H_2O due to its shorter excited state lifetime [47]. For consistency in estimating the coherence decay by use of Eq. (19), we chose 100 excited state configurations from the D_2O trajectories at the same times ($\geq$ 1 ps) that we used for the H_2O trajectories.

Fig. 4 shows a comparison of the nuclear decay function $J(t)$ for the solvated electron in H_2O and in D_2O, calculated from Eqs. (19) and (34). The coherence decay in D_2O is qualitatively similar to that in H_2O, only for D_2O the approximate Gaussian decay time is $\approx$ 5.6 fs (versus $\approx$ 4.5 fs for H_2O). We note that the results in this figure are not in good agreement with the previous work of Neria and co-workers [20,21] who found almost identical coherence decays for the electron in H_2O and D_2O. This finding played a role in our choice of identical coherence time for the electron in H_2O and D_2O; see [47]. Although we cannot be sure, the difference may

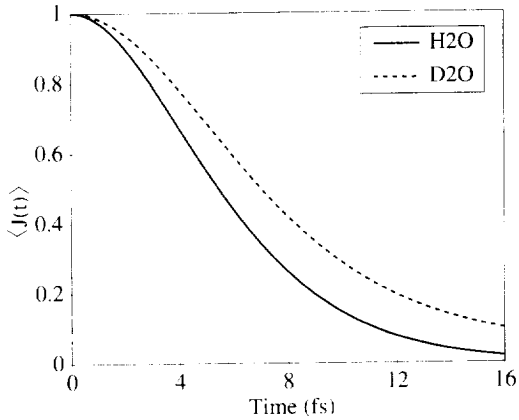

Fig. 4. The isotope effect on quantum decoherence. The solid line shows the full decay of quantum coherence for the hydrated electron. The dashed line shows the full decay of quantum coherence for the solvated electron in D_2O. The isotope effect slows the coherence decay in heavy water by $\approx$ 25%; see text for details.

reflect the result of statistical fluctuations in the data of Neria and co-workers. To evaluate the non-adiabatic transition rate, Neria and co-workers utilized a time-dependent form for the golden rule transition rate which required running trajectories on both electronic surfaces [20,21], but as such trajectories are costly, they limited their ensemble to only 15 examples. With our short time approximation, we were able to easily include 100 examples in the determination of the coherence decay. When we mimicked their calculation by selecting different subsets of only 15 examples for the ensemble average, we found coherence decays that varied by nearly a factor of 3. This suggests that insufficient statistics may have played a role in their result of identical coherence decays for the two fluids.

The longer coherence time in heavy water compared to light water arises predominantly from the difference in mass in the choice of the Gaussian width (Eq. (34). For classical H_2O and D_2O, the probability of a given nuclear configuration is the same. Static ensemble properties for the two fluids should be identical since the ensembles contain identical nuclear configurations with equal statistical weights. Real (quantum mechanical) water and heavy water have slightly different properties, however, primarily due to the difference in spatial dispersion between the proton and the deuteron (see for example [48]). Since the electronic Hamiltonian for the solvated

electron is identical for both heavy and light water, the static ensemble averaged potential energy difference and the difference in Hellmann–Feynman forces on the two surfaces will also be identical for the two fluids. Thus, the only difference in the evaluation of the coherence decay for the two fluids via Eq. (19) is in the mass term that enters through the Gaussian width in Eq. (34). Since the nuclear overlap part of the coherence decay depends on the sum over nuclei, the mass change leads to the net slower decay of coherence in D_2O versus H_2O. In fact, for the purposes of evaluating $J(t)$ for the solvated electron in D_2O, the H_2O simulations would suffice.

The different coherence decay times in the two solvents play a direct role in determining the isotope effect on the overall non-adiabatic transition rate. In simplified terms, to determine the non-adiabatic transition rate before quantum coherence has decayed, non-adiabatic transition *amplitudes* should be added; after the decoherence interval, memory of the complex phases is lost and non-adiabatic transition *probabilities* should be added. This view can be used to estimate non-radiative transition rates in limiting cases. During the course of the non-adiabatic simulations described above, the probability of making an electronic transition at a given time step was strictly determined by the square of the appropriate non-adiabatic transition amplitude, a direct consequence of the choice to keep coherence for only one time step. Thus, the non-adiabatic transition rate, or probability of making the transition per unit time in this "incoherent" limit, is given by the sum of the squares of the non-adiabatic transition amplitudes:

$$P_{ij}(\Delta t) = \frac{1}{\Delta t}\left\langle \sum_{n=1}^{\tau} |T_{ij}(\Delta t)|^2 \right\rangle \tag{35}$$

In Eq. (35), $P_{ij}(\Delta t)$ is the probability per unit time of making a non-adiabatic transition between states i and j averaged over τ time steps along a trajectory in the limit of keeping coherence for only one time step (Δt). The τ consecutive transition amplitudes, $T_{ij}(\Delta t)$, are given by Eq. (16), and the angled brackets indicate an ensemble average over starting times and trajectories.

If coherence were maintained over several consecutive time steps, $n\Delta t$, the complex transition amplitudes would first be summed over those time steps, allowing for interference, and then the square would be taken to determine the non-adiabatic transition probability per unit time.

$$P_{ij}(\tau) = \frac{1}{Q}\sum_{N}\frac{1}{\tau}\omega_N(\tau, n\Delta t)\left|\sum_{n=1}^{\tau} T_{ij}^{(N)}(n\Delta t)\right|^2 \tag{36}$$

Here, $P_{ij}(\tau)$ is the probability of making a non-adiabatic transition between states i and j per unit time where coherence is completely maintained for τ consecutive time steps. $T_{ij}^{(N)}(n\Delta t)$ is the non-adiabatic transition amplitude at the nth time step starting from the Nth configuration. In other words, we propagate the quantum subsystem coherently over the coherence time which is picked from a distribution of possible coherence times. Once coherence has been lost, the possible quantum paths become course grained and we can begin to add probabilities. The outer summation is over starting configurations and the weights refer to the statistical probability of a given configuration having a coherence time of τ. The weights, $w_N(\tau,n\Delta t)$, are the statistical probabilities that the Nth run will have maintain coherence for $n\Delta t$ time steps given that the characteristic coherence time is τ. These weights are normalized by Q. Thus, the complex transition amplitudes from previous simulations which utilized shorter coherence times can be used to determine what the non-adiabatic transition rate would have been if quantum coherence were retained over an arbitrary number of time steps. Comparison of non-adiabatic transition probabilities determined from Eqs. (35) and (36) as a function of the characteristic coherence time provides a direct measure of the influence of coherence on non-adiabatic transition rates.

Fig. 5 displays the average lifetime for remaining in the equilibrium excited state, $\langle\tau_{ex}\rangle$ computed as a function of the coherence time for the solvated electron in both H_2O and D_2O. These lifetimes are averaged over 3000 starting configurations drawn from the 5 longest trajectories at times past 1 ps. The average probability per unit time of leaving the excited state for the electron in D_2O is approximately 1.2 parts per thousand while that for the hydrated electron is roughly half again as large. For a 1 fs time step, these average lifetimes correspond to $\approx$ 550 fs in H_2O and $\approx$ 850 fs in D_2O. The magnitudes of these rates agree reasonably with the rates obtained from fits to the actual population decays in the

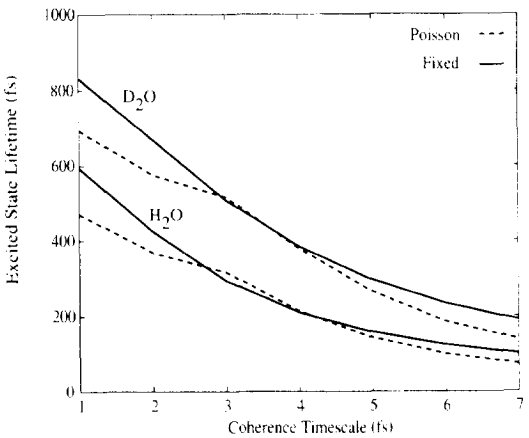

Fig. 5. Effect of quantum decoherence on the excited state lifetime of the hydrated electron. The dashed and solid curves show the corresponding "coherent" products of the non-adiabatic transition amplitudes in light and heavy water, respectively. The "coherent" and "incoherent" transition probabilities are identical for 1 fs coherence time due to the simulation algorithm.

simulations and the $\approx$ 2:1 simulated isotope effect between D_2O and H_2O [47] is adequately reproduced.[6] As discussed elsewhere, non-adiabatic transitions usually occur from those configurations with somewhat higher than average transition probabilities or lower than average survival probabilities [46]. These special configurations, however, occur with a low enough frequency that the average transition probability provides a reasonable estimate of the non-equilibrium population dynamics.

Fig. 5 shows the average excited state lifetimes for remaining in the excited state for the solvated electron in heavy and light water, respectively, computed as a function of the coherence time τ ($P_{22}(\tau)$, Eq. (36). Here, coherence was maintained for exactly the same amount of time in each sample, Thus, the normalized weights for each sample run are given by

$$\omega_N(\tau, n\Delta t)/Q = \delta(\tau - n\Delta t) \tag{37}$$

For a coherence time τ = 1 fs, these curves coincide exactly with those computed from Eq. (35), as expected. For coherence times longer than 1 fs, constructive interference between the transition amplitudes at consecutive time steps leads to a significant lowering of the survival probability per unit time – in other words, increasing the quantum coherence time increases the likelihood for making a non-adiabatic transition. The magnitude and phase of the non-adiabatic coupling in this system do not vary much on the time scale of a few femtoseconds, so that changes in the coherence time result directly in changes in the electronic transition rate in this "incoherent" limit.

Fig. 5 also compares the effect of using different distributions of coherence times to compute the excited state lifetimes. Here, we chose the coherence time for each averaged run from a Poisson (exponential) distribution of possible coherences times. As mentioned above, introducing a distribution of coherence times is consistent with statistical treatments of quantum dissipation/decoherence. The x-axis here is thus the "characteristic" coherence timescale for the Poisson (exponential) probability distribution function of coherence times. The normalized weights are computed using

$$\omega_N(\tau, n\Delta t)/Q = \exp(-n\Delta t/\tau)/\tau \tag{38}$$

The close agreement between the exponentially distributed (Poisson) data and the single coherence time data provides a good check on the robustness of using a single decoherence time to approximate a distribution of coherence times. This is being used to guide further investigations into this system and others.

Armed with the coherence decay times for both H_2O and D_2O from Fig. 4, we can make use of the coherence time dependence of the excited state lifetimes displayed in Fig. 5 to provide a revised estimate of the isotope effect. For equal coherence decay times, as in the original ansatz in the simulations by Schwartz and Rossky, the survival probabilities in Fig. 5 predict a roughly 2:1 isotope effect in the non-adiabatic transition rate between D_2O and H_2O. This is a direct reflection of smaller non-adiabatic coupling in D_2O due to smaller nuclear velocities. However, for a decoherence time in D_2O which is roughly 25% longer than that in H_2O, the present method of estimation yields non-adiabatic transition rates in the two solvents which are identical to within 20%. For example, choosing the areas under the $J(t)$ curves as estimates of the decoherence times, we

[6] A simple model assuming the non-adiabatic transition probability is inversely proportional to the quantum energy gap allows for an estimation of the transition rate from the equilibrium excited state (see [29,47]). The rates were estimated from the population dynamics in the simulations to be 450 fs^{-1} for H_2O and 850 fs^{-1} for D_2O.

obtain predicted lifetimes for the equilibrium excited state of the solvated electron of 200 and 250 fs in H_2O and D_2O, respectively (see Fig. 5). This result provides a microscopic explanation for the lack of isotope effect observed in the femtosecond experiments: the smaller non-adiabatic coupling in D_2O adds coherently for a longer time than that in H_2O; the two opposing effects nearly cancel for this system, leading to a non-intuitively small isotopic dependence of the non-adiabatic transition rate.[7] Furthermore, the rates reported here agree with the experimentally determined relaxation rate 310 ± 80 fs reported by Barbara's group [35]. Although the absolute transition rate constants are difficult to predict from simulation,[8] Fig. 5 provides a clear demonstration that quantum decoherence plays a direct role in the electronic dynamics of this very important condensed-phase chemical system.

4. Discussion

In conclusion, we have presented a theory based upon the consistent or decoherent histories interpretation of quantum mechanics to provide a suitable mechanism and explanation for the destruction of quantum phase coherence in non-adiabatic quantum molecular dynamics. We have illustrated in two examples chosen from condensed-phase chemical dynamics the important role of quantum decoherence. Moreover, we have demonstrated the profound sensitivity of quantum mechanical lifetimes to the quantum coherence time. As the coherence timescale is reduced, the quantum system cannot form long-lived superpositions of states and the excited state populations are diminished. This gives rise to a return to adiabatic dynamics when the coherence timescale is sufficiently short and the coupling between the quantum and classical variables is large. This effect of "frictional" damping of non-adiabatic effects may play a key role in electron transfer reaction in many important biological processes such as photosynthesis, oxidative phosphorylation and redox reactions.

[7] Note that since the solvation dynamics take place on slightly different timescales in the two solvents, there would still be some minor differences in the observed transient spectroscopy. A spectral calculation based on the simulations which assumes identical non-adiabatic transition rates for H_2O and D_2O shows that at 300 fs time resolution, however, there would be little observable isotope effect (see [47]).

[8] There are many issues in trying to determine the absolute magnitude of the non-adiabatic transition rate from simulations, the chief difficulty lying in the classical treatment of the solvent. For systems where the non-adiabatic coupling is linear in the spectral density of the bath, it is possible to make a "quantum correction" based on detailed balance and other factors to the semi-classically determined rate [49]. These correction factors are not appropriate for the hydrated electron, however, as the non-adiabatic coupling is spread out throughout the solvent (see [46]) so that there is a distinctly non-linear relationship between the coupling and the solvent spectral density.

Acknowledgements

This work was supported by a grant from the National Science Foundation. Both E.R.B. and B.J.S. gratefully acknowledge the support of National Science Foundation Postdoctoral Fellowships in Chemistry.

References

[1] (a) A. Staib, D. Borgis and J.T. Hynes, J. Chem. Phys., 102 (1995) 2487; J.M. Papanikolas, P.E. Maslen and R. Parson, J. Chem. Phys., 102 (1995) 2452.(b) D. Thirumalai, E.J. Bruskin and B.J. Berne, J. Chem. Phys., 83 (1985) 230; A. Selloni, R. Car, M. Parinello and P. Carnevali, J. Phys. Chem., 91 (1987) 4947; M. Sprik and M.L. Klein, J. Chem. Phys., 89 (1988) 1592.

[2] (a) D.F. Coker, in M.P. Allen and D.J. Tildesley (Eds.), Computer Simulations in Chemical Physics, Kluwer Academic, Dordrecht, 1993, p. 315 and references cited therein. (b) S. Hammes-Schiffer and J.C. Tully, J. Phys. Chem., 99 (1995) 5793; L. Xiao and D.F. Coker, J. Chem. Phys., 102 (1995) 1107 as well as Refs. 21–23.

[3] A. Garg, J.N. Onuchic and V. Ambegaokar, J. Chem. Phys., 83 (1985) 4491; J.N. Onuchic, J. Chem. Phys., 86 (1987) 3925 and references cited therein.

[4] P.G. Wolynes, J. Chem. Phys., 86 (1987) 1957.

[5] E.R. Bittner and P.J. Rossky, J. Chem. Phys., 103 (1995) 8130.

[6] J.C. Tully and R.K. Preston, J. Chem. Phys., 55 (1971) 562.

[7] J.C. Tully, J. Chem. Phys., 93 (1990) 1061.

[8] F.A. Webster, J. Schnitker, M.S. Friedrichs, R.A. Friesner and P.J. Rossky, Phys. Rev. Lett., 66 (1991) 3172; F.A. Webster, P.J. Rossky and R.A. Friesner, Comput. Phys. Commun., 63 (1991) 494.

[9] F.A. Webster, E.T. Wang, P.J. Rossky and R.A. Friesner, J. Chem. Phys., 100 (1994) 4835.

[10] T.H. Murphrey and P.J. Rossky, J. Chem. Phys., 103 (1995) 6665.

[11] D.F. Coker and L. Xiao, J. Chem. Phys., 102 (1995) 496 and references cited therein.

[12] R.B. Griffiths, J. Stat. Phys., 36 (1984) 219.
[13] R. Omnés, Ann. Phys., 201 (1989) 354.
[14] R. Omnés, Rev. Mod. Phys., 53 (1992) 893.
[15] M. Gell-Mann and J.B. Hartle, Quantum mechanics in the light of quantum cosmology, in W.H. Zurek (Ed.), Complexity, Entropy and the Physics of Information, Addison-Wesley, Redwood City, CA, 1990.
[16] M. Gell-Mann and J.B. Hartle, Phys. Rev. D, 47 (1993) 3345.
[17] S. Okazaka, J. Wang and P.G. Wolynes, Personnel communication (1995).
[18] P. Pechukas, Phys. Rev., 181 (1969) 174.
[19] E.J. Heller, J. Chem. Phys., 75 (1981) 2923.
[20] E. Neria, A. Nitzan, R.N. Barnett and U. Landmann, Phys. Rev. Lett., 67 (1991) 1011.
[21] E. Neria and A. Nitzan, J. Chem. Phys., 99 (1993) 1109.
[22] H. Hellmann, Einführung in die Quantenchemie, Deuticke, Leipzig, 1937.
[23] R.P. Feynmann, Phys. Rev., 56 (1939) 340.
[24] A.O. Caldeira and A.J. Leggett, Ann. Phys., 149 (1983) 374.
[25] G. Lindblad, Commun. Math. Phys., 48 (1976) 119.
[26] A Staib and D. Borgis, J. Chem. Phys., 103 (1995) 2642. This paper describes a semi-classical Golden Rule approach to non-adiabatic transition rates which captures elements of the quantum statistics of the bath.
[27] B.J. Schwartz, E.R. Bittner, O.V. Prezhdo and P.J. Rossky, J. Chem. Phys., 104 (1996) 5942.
[28] E.R. Bittner and P.J. Rossky, in preparation.
[29] B.J. Schwartz and P.J. Rossky, J. Chem. Phys., 101 (1994) 6902, 6917; D. Borgis and A. Staib, Chem. Phys. Lett., 230 (1994) 405.
[30] B.J. Schwartz and P.J. Rossky, J. Phys. Chem., 98 (1994) 4489; 99 (1995) 2953; Phys. Rev. Lett., 72 (1994) 3282.
[31] T.H. Murphrey and P.J. Rossky, J. Chem. Phys., 99 (1993) 515.
[32] R.B. Barnett, U. Landmann and A. Nitzan, J. Chem. Phys., 90 (1989) 4413.
[33] E. Keszei, S. Nagy, T.H. Murphrey and P.J. Rossky, J. Chem. Phys., 99 (1993) 2004; E. Keszei, T.H. Murphrey and P.J. Rossky, J. Phys. Chem., 99 (1995) 22.
[34] P.J. Rossky and J. Schnitker, J. Phys. Chem., 92 (1988) 4277 and references cited therein.
[35] J.C. Alfano, P.K. Walhout, Y. Kimura and P.F. Baxbaxa, J. Chem. Phys., 98 (1993) 5996; Y. Kimura, J.C. Alfano, P.K. Walhout and P.F. Barbara, J. Phys. Chem., 98 (1994) 3450; P.K. Walhout and P.F. Baxbara, personal communication, (1995).
[36] P.J. Reid, C. Silva, P.K. Walhout and P.F. Barbara, Chem. Phys. Lett., 228 (1994) 658.
[37] F.H. Long, H. Lu and K.B. Eisenthal, Phys. Rev. Lett., 64 (1990) 1469; F.H. Long, H. Lu, X. Shi and K.B. Eisenthal, Chem. Phys. Lett., 185 (1991) 47 and references cited therein.
[38] A. Migus, Y. Gauduel, J.L. Martin and A. Antonetti, Phys. Rev. Lett., 58 (1987) 1559; S. Pommeret, A. Antonetti and Y. Gauduel, J. Am. Chem. Soc., 113 (1991) 105.
[39] F.H. Long, H. Lu and K.B. Eisenthal, Chem. Phys. Lett., 160 (1989) 464; Y. Gauduel, S. Pommeret, A. Migus and A. Antonetti, J. Phys. Chem., 95 (1991) 533.
[40] J.L. McGowen, H.M. Ajo, J.Z. Zhang and B.J. Schwartz, Chem. Phys. Lett., 231 (1994) 504.
[41] M.U. Sander, K. Luther and J. Troe, Ber. Bunsenges. Phys. Chem., 97 (1993) 953 and references cited therein.
[42] P.J. Rossky and J.D. Simon, Nature, 370 (1994) 263.
[43] K. Toukan and A. Rahman, Phys. Rev. B, 31 (1985) 2643.
[44] J. Schnitker and P.J. Rossky, J. Chem. Phys., 86 (1987) 3462.
[45] M.P. Allen and D.J. Tildesley, Computer Simulations of Liquids, Oxford University Press, New York, 1987.
[46] O.V. Prezhdo and P.J. Rossky, J. Phys. Chem, 100 (1996) 17094.
[47] B.J. Schwartz and P.J. Rossky, J. Chem. Phys., 105 (1996) 6997.
[48] G.S. Delbuono, P.J. Rossky and J. Schnitker, J. Chem. Phys., 95 (1991) 3728.
[49] J.S. Bader and B.J. Berne, J. Chem. Phys., 100 (1994) 8359.